Asian Journal of Chemistry; Vol. 37, No. 11 (2025), 2781-2793
ASIAN JOURNAL OF CHEMISTRY
https://doi.org/10.14233/ajchem.2025.34580

Adsorption of Crystal Violet onto Agricultural Waste-Derived Biosorbents: A Study of Isotherm, Kinetic and Thermodynamic Behaviours

M.S.I. ROPAK, M.A. NOPUR, M.F. SHIKDER and U. SALMA*,

Department of Chemistry, Mawlana Bhashani Science and Technology University, Santosh, Tangail-1902, Bangladesh

*Corresponding author: Phone: +88 01608257719; E-mail: ummesalma@mbstu.ac.bd

Received: 30 July 2025 *Accepted*: 25 September 2025 *Published online*: 27 October 2025 AJC-22167

Developing sustainable and economically viable removal approaches is crucial, due to the rampant use of synthetic dyes, such as crystal violet, in effluent poses significant environmental and health hazards. To remove crystal violet from aqueous medium, this work emphasizes the application of three inexpensive biosorbents, namely tea waste (TW), rice husk (RH) and sugarcane bagasse (SCB). The functional and structural properties of the biosorbents were determined using FTIR, FE-SEM, pHpzc analysis, XRD and BET surface area measurements. To optimize the experimental parameters, batch adsorption experiments were performed at an initial concentration of 40 ppm of dye, a biosorbent dosage of 1 g/L, a solution pH of 9 and a temperature of 30 ºC, which resulted in maximum adsorption efficiency. Analysis of the isotherm data showed that crystal violet adsorption predominantly followed the Langmuir model. The biosorbents SCB, RH and TW exhibited the maximum adsorption capacities (q_m) of 61.35, 58.82 and 53.19 mg/g, respectively. Kinetic results indicated a strong correlation with the pseudo-second-order model, implying that chemical interactions played a significant role in the adsorption process. The research illustrates that TW, RH and SCB are simple, affordable, readily available and efficient options for use as biosorbents in wastewater treatment.

Keywords: Biosorbent, Adsorption, Wastewater treatment, Crystal violet dye, Thermodynamic analysis, Equilibrium studies.

INTRODUCTION

Water is a cornerstone of human civilization, supporting agriculture, transportation, sanitation and industry. However, water pollution has become a critical global issue due to industrialization, urbanization and agricultural activities [1]. As the global population grows, access to safe water continues to diminish, with nearly 1.8 billion people projected to face absolute water scarcity by 2025 [2]. Addressing this challenge requires the efficient treatment of industrial wastewater to remove contaminants before environmental release.

Dye pollution is a primary concern, with industries such as textiles, dyeing, cosmetics, food and leather releasing large quantities of wastewater containing toxic dyes [3]. An annual discharge of nearly 700,000 tons of synthetic dyes occurs worldwide [4]. Industrial dyes are typically categorized by charge into three main types: cationic or basic dyes, anionic dyes like direct, acid and reactive types and non-ionic disperse dyes. Cationic dyes pose the greatest environmental risk due to their high toxicity [5]. Among these, crystal violet, a triphenylmethane cationic dye, is extensively used in pharmaceuticals, textiles and printing industries [6]. When released into water, crystal violet reduces sunlight penetration, disrupts photosynthesis [7] and poses significant health risks to aquatic organisms and humans including respiratory issues, skin irritation and potential mutagenicity [6]. This underscores the urgent need to remove crystal violet dye from wastewater prior to its release into the environment.

Various methods, including reverse osmosis, chemical oxidation, nanofiltration, photocatalysis and biological degradation, have been investigated to eliminate dyes from aqueous media, ensuring reduced contamination [5]. Among them, biological treatment processes are inefficient due to the non-biodegradability of dyes [8]. The chemical dye removal process often has a high cost or technical challenges and is rarely used in actual applications [8]. Adsorption, by contrast, stands out as an economically viable, efficient and environmentally friendly method for dye removal [5]. Transforming agricultural byproducts into adsorbents further reduces preparation costs and offers a sustainable alternative to waste disposal

methods like burning [9]. Sugarcane bagasse (SCB), a byproduct of the sugarcane industry, is produced in significant quantities, with global production estimated at 700 million tons annually [10]. SCB primarily contains cellulose (34-46%), hemicellulose (22-32%), lignin (17-30%) and ash (1-8%) [11]. Its low cost, abundance and porous nature make it an excellent adsorbent [12]. Similarly, rice husk (RH), a byproduct of rice milling, is produced worldwide, with global rice production exceeding 190 million tons as of 2016 [13]. RH is a lignocellulosic material consisting of 32% cellulose**,** 21% of both hemicelluloses and lignin, 20% ash, which is rich in silica (SiO_2, 85-95%) and 3% crude proteins, making it ideal for adsorption, biochar production and silica-based composites [13]. Tea waste (TW) is another agricultural byproduct with an annual global production of 5.8 million metric tons in 2018 [14]. Its typical composition includes 20-30% cellulose, 5-15% hemicellulose, 15-30% lignin, 15-20% proteins and 5-10% polyphenols, enhancing its adsorption capabilities [14]. Utilizing SCB, RH and TW as biosorbents offers a sustainable and cost-effective approach to environmental remediation.

So, this study aims to remove crystal violet dye from textile wastewater and compare the adsorption capacities of SCB, RH and TW as low-cost biosorbents. The biosorbents were characterized using XRD, FTIR, SEM, pHpzc and N_2 adsorption-desorption isotherm analysis. Batch adsorption experiments were performed to evaluate the impact of biosorbent dosage, initial dye concentration, temperature and dye solution pH. Furthermore, the study examined the interactions between crystal violet dye and the biosorbents by assessing the adsorption isotherm, kinetics and thermodinamic parameters.

EXPERIMENTAL

Preparation of biosorbents: The biosorbents tea waste (TW), rice husk (RH) and sugarcane bagasse (SCB) were sourced from a local market in Tangail, Bangladesh. At first, they were rinsed under running tap water, followed by deionized water, to eliminate sugar residues, clay and dirt particles. For the preparation of tea waste powder, it was further boiled with deionized water for 1 h to remove any residual colour, pigments and tannins. These materials were dried at 85 ºC, ground by a grinding machine and passed through a 75-micron sieve. The final biosorbents were kept in a desiccator for subsequent application.

Characterization: The prepared biosorbents underwent detailed characterization through several advanced characterization methods like X-ray diffraction (XRD), Fourier transform infrared (FTIR) spectroscopy and field-emission scanning electron microscopy (FE-SEM), point of zero charge (pHpzc) and BET N_2 adsorption-desorption analysis. Detailed methodologies for these characterizations are provided in our recently published article [11].

Preparation of crystal violet dye solution: Crystal violet dye was sourced from SRL (India) and utilized without further purification. By dissolving 0.05 g of crystal violet in 500 mL of deionized water, a stock dye solution with a concentration of 100 ppm was prepared. The appropriate dilutions of the stock solution were prepared as needed just before the adsorption experiments were performed. The pH of the dye solution was adjusted using 0.1 M NaOH or HCl to prepare the desired experimental conditions.

Adsorption experiments: Optimization experiments for crystal violet removal were done using varying biosorbent dosages, contact periods, dye solution pH, temperature and initial concentrations. In each experiment, 15 mL dye solution was mixed with the biosorbent in a vial, stirred at 300 rpm and analyzed *via* UV-visible spectroscopy. Each experiment was conducted in triplicate and the results are presented as the mean ± standard deviation. The adsorption efficiency (%) was calculated using eqn. 1:

$$\text{Adsorption efficiency (\%)} = \frac{C_o - C_e}{C_o} \times 100 \quad (1)$$

where C_o and C_e (mg/L) denote the initial concentration and residual concentration at time t of crystal violet, respectively. Besides, the adsorption capacity at the specific time (q_t) and equilibrium (q_e) were determined using eqns. 2 and 3, respectively:

$$q_t = (C_o - C_t) \times \frac{V}{m} \quad (2)$$

$$q_e = (C_o - C_e) \times \frac{V}{m} \quad (3)$$

where C_t (mg/L) denotes the residual concentration at time t of crystal violet; V (L) denotes the dye solution's volume; and m (g) represents the adsorbent's quantity used.

RESULTS AND DISCUSSION

Characterization of the biosorbents

XRD analysis: The XRD profiles of the synthesized biosorbents are presented in Fig. 1. The lack of sharp diffraction peaks across all samples highlights their predominantly amorphous nature, attributed to the high content of lignin, hemicellulose and ash [15]. This amorphous structure enhances the suitability for biosorption by allowing rapid penetration of dye molecules onto the surface [16]. In Fig. 1a, sugarcane bagasse (SCB) displays characteristic XRD peaks at 15.5º, 21.8º and 34.8º, corresponding to the lattice planes of type I cellulose [11]. Similarly, the XRD pattern of rice husk (RH) in Fig. 1b shows typical crystallization peaks at 15.6º, 22º and 34.8º, reflecting type I cellulose [17]. More-over, the peak at 20.9º is associated with silica (SiO_2) [18], a significant component of RH. In Fig. 1c, tea waste (TW) exhibits a broad peak centered at 20.9º, indicating an essentially amorphous structure [19]. Amorphous lignin and hemicellulose are responsible for this behaviour, as they interfere with the crystalline nature of cellulose.

Segal's method was employed to determine the crystallinity index (CrI) of the biosorbents [20,21]:

$$\text{CrI (\%)} = \frac{I_{002} - I_{am}}{I_{002}} \times 100 \quad (5)$$

where I_{002} is the maximum intensity of the crystalline peak corresponding to the (200) plane and I_{am} is the minimum intensity of the amorphous region. The crystallite size of the biosorbents was estimated through the Scherrer formula [22]:

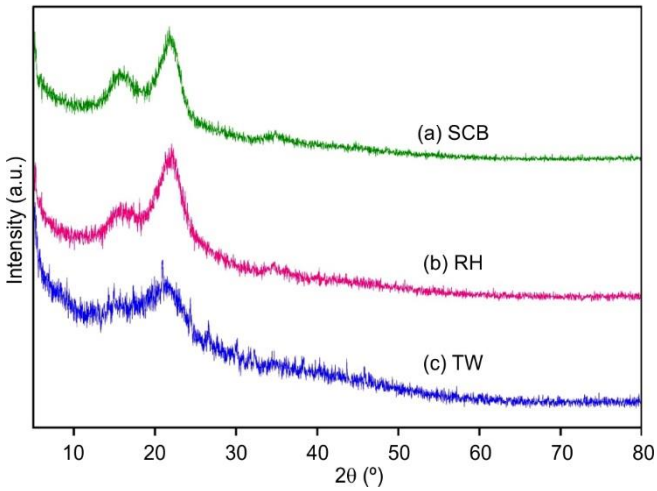

Fig. 1. XRD patterns of the prepared biosorbents: (a) sugarcane bagasse, (b) rice husk and (c) tea waste

$$D = \frac{k\lambda}{\beta \cos\theta} \quad (6)$$

where D represents the crystallite size (nm), λ is the wavelength of X-ray (0.154 nm), k is the Scherrer constant (0.90), β is the FWHM (full width at half maximum) of the peak in radians and θ is the corresponding Bragg angle (°).

Table-1 summarizes the structural and crystallographic parameters of the biosorbents. The crystallinity index indicates the degree of order, with RH being the most crystalline due to silica, SCB semi-crystalline and TW predominantly amorphous. Crystallite size follows a similar trend, with SCB and RH larger than TW, reflecting the more disordered nature of TW.

FE-SEM analysis: Fig. 2a-b depicts the surface of sugarcane bagasse (SCB) with distinct longitudinal grooves and ridges, indicative of cellulose microfibrils [32]. The relatively smooth surface suggests minimal surface modifications [24]. Fig. 2c-d highlights the micrographs of rice husk (RH), revealing a rigid structure with sharp edges and silica-rich deposits, confirming its composition of cellulose and silica [20]. The presence of irregular particle fragments on the surface enhances its roughness, which is advantageous for adsorption [25]. In tea waste (TW), the surface has a rough, porous and uneven structure with visible cavities (Fig. 2e-f). This irregular surface, mainly due to components like cellulose and hemicellulose, helps improve its adsorption properties [26].

FT-IR analysis: Fig. 3 shows the FT-IR spectra of SCB, RH and TW, indicating that the functional groups are actively involved in the adsorption. The broad absorption around 3400 cm^{-1} in all samples is associated with the hydroxyl (O–H) stretching mode, suggesting the presence of cellulose, hemi-

TABLE-1
CRYSTALLOGRAPHIC PARAMETERS OF BIOSORBENTS DERIVED FROM XRD ANALYSIS

Biosorbent	2θ (°)	Crystallinity index, CrI (%)	Crystallite size, D (nm)	Amorphous/Crystalline nature
SCB	15.5, 21.8, 34.8	55.43	20.88	Semi-crystalline
RH	15.6, 20.9, 22, 34.8	56.25	18.40	Crystalline with silica
TW	20.9	37.31	13.2	Predominantly amorphous

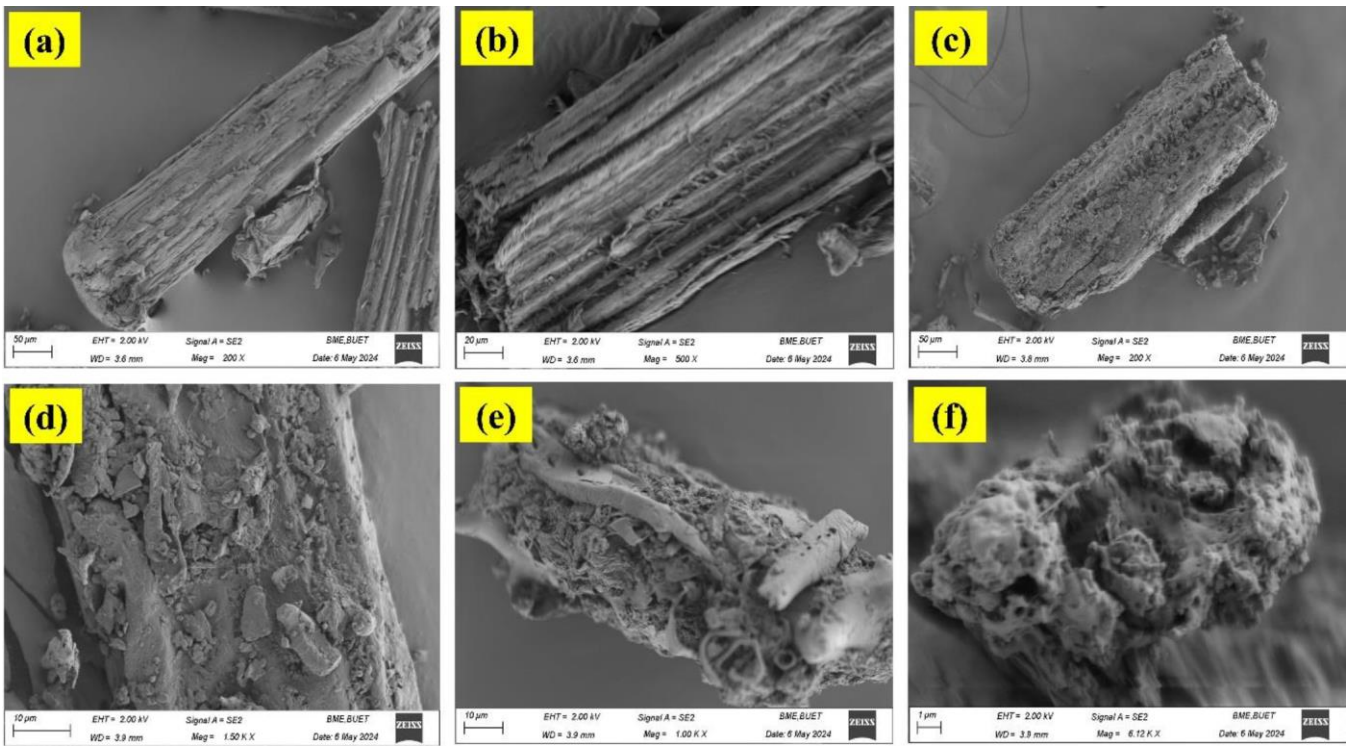

Fig. 2. FE-SEM images of the prepared biosorbents: (a,b) sugarcane bagasse, (c,d) rice husk and (e,f) tea waste

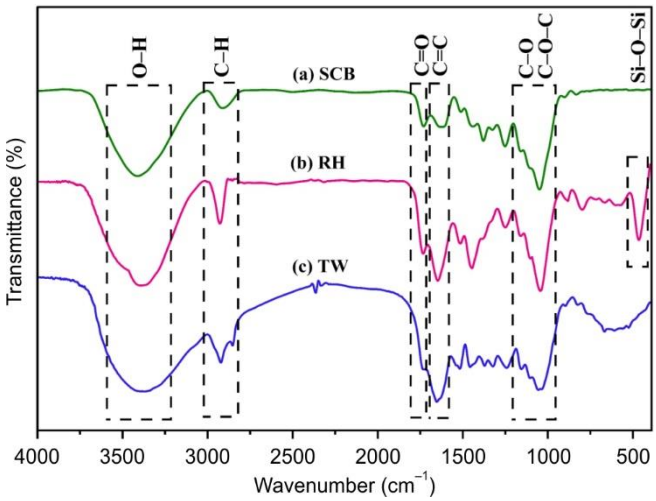

Fig. 3. FT-IR analysis of the prepared biosorbents: (a) sugarcane bagasse (SCB), (b) rice husk (TH) and (c) tea waste (TW)

cellulose and lignin. Peaks near 2900 cm^{-1} are attributed to the aliphatic C–H stretching [25,26], whereas the weaker band observed at 1735 cm^{-1} is attributed to the C=O stretching vibrations of carboxyl and ester groups present in hemicelluloses [11]. The peaks within 1650-1600 cm^{-1} are attributed to the aromatic C=C or carboxyl groups [27]. The bands at 1091 cm^{-1} and 1041 cm^{-1} are linked to C–O stretching or C–O–C stretching of cellulose, hemicellulose and lignin [28]. A peak at 469 cm^{-1}, corresponding to Si–O–Si bending, is particularly prominent in RH due to its high silica content [25,29]. For TW, the presence of aromatic and phenolic groups is confirmed by peaks in the 1600-1500 cm^{-1} region, contributing to its adsorption properties [30,31].

BET-based surface area and porosity analysis: The characterization of surface area and pore size using BET analysis provides insights into the textural properties of SCB, RH and TW, as depicted in Fig. 4. All the biosorbents show type IV isotherms with hysteresis loops of H3-type, indicative of mesoporous structures according to IUPAC classification [32]. The IUPAC further categorizes pores by diameter into micropores (< 20 Å), mesopores (20-500 Å) and macropores (> 500 Å) [33,34]. According to the pore size distribution derived from the BJH method, most biosorbent pores fall within the mesoporous range. However, TW exhibits a broader pore size distribution with contributions from macropores, which improve the accessibility but lower the adsorption density. Table-2 summarizes the textural properties, where SCB stands out with the highest BET surface area (87.86 m^2/g), pore volume (0.1113 cc/g) and an average pore diameter of 50.69 Å, highlighting its potential as the most efficient adsorbent among the samples. Tea waste (TW) shows slightly better textural properties than RH, featuring a surface area (BET) of 9.31 m^2/g, a total pore volume amounting to 0.0157 cc/g and an average pore diameter expanded to 67.59 Å. Overall, SCB outperforms RH and TW due to its superior surface area and well-developed mesoporosity [35].

TABLE-2
BET PARAMETERS OF THE PREPARED BIOSORBENTS

Biosorbent	BET surface area (m^2/g)	Pore volume (cc/g)	Pore diameter (Å)
Rice husk	8.03	0.0108	53.85
Sugarcane bagasse	87.86	0.1113	50.69
Tea waste	9.31	0.0157	67.59

Optimization of adsorption parameters

Contact time: In adsorption studies, contact time is an essential parameter, as it determines the equilibrium period and adsorption efficiency of the biosorbent [36]. The adsorption behaviour of crystal violet over varying contact times, up to 60 min, is shown in Fig. 5. A rapid enhancement in removal efficiency and adsorption capacity was observed for all the three biosorbents at the beginning of the contact time (5-20 min). SCB exhibited the highest removal efficiency, reaching 93.9 ± 0.5% at 60 min, while RH and TW reached 92.9 ± 0.7% and 90.5 ± 0.8%, respectively. The adsorption capacity followed a similar trend, with SCB achieving 37.6 ± 0.4 mg/g, RH 37.1 ± 0.7 mg/g and TW 36.7 ± 0.6 mg/g at 60 min. The slight increase in removal efficiency and adsorption capacity beyond 40 min indicates nearing saturation, suggesting equilibrium is reached around 30-40 min. This is because, initially, the availability of several vacant binding sites promotes the rapid crystal violet uptake, but as these sites become saturated, the adsorption rate decreases [36,37]. The higher adsorption performance of SCB can be ascribed to its greater surface area and active sites compared to RH and TW, which facilitates enhanced dye uptake.

Biosorbent dosage: Optimizing biosorbent dosage is an essential aspect of making the overall adsorption process more economical [37]. Increasing the biosorbent dosage from 0.5 to 2 g/L resulted in enhanced crystal violet removal efficiency across all biosorbents, with SCB reaching 97.4 ± 1.2%, RH 97.9 ± 1.3% and TW 96.1 ± 1.1% (Fig. 6). However, the rate of improvement diminished beyond a certain point, indicating that further increases in dosage resulted in minimal gains in dye removal. Therefore, an optimum dosage of 1 g/L was chosen for subsequent adsorption studies for all biosorbents. Conversely, the adsorption capacity (mg/g) decreased with increasing dosage from 0.5 to 2 g/L; SCB decreased from 72.2 ± 0.9 to 19.5 ± 1.4 mg/g, RH from 71.2 ± 0.8 to 18.3 ± 1.5 mg/g and TW from 68.2 ± 0.8 to 16.1 ± 1.4 mg/g. Mondal *et al.* [38] also reported a similar observation regarding removing Congo red by banana peel dust. This trend suggests that higher biosorbent dosages increase the availability of active sites and enhance removal efficiency. However, they also cause particle aggregation, reducing the effective surface area per unit mass and subsequently lowering adsorption capacity [37].

Initial concentration of dye solution: Another parameter impacting adsorption efficiency is the concentration of the dye solution [37]. The adsorption behaviour of SCB, RH and TW varies with the initial concentration of CV, as shown in Fig. 7. A slight decrease in removal efficiency was observed for all biosorbents, with an increase in dye concentration from 20 to 50 mg/L: SCB dropped from 96.1 ± 1.2% to 90.9 ± 1.2%, RH from 96.9 ± 1.1% to 88.9 ± 0.7% and TW from 96.0 ± 0.8% to 85.2 ± 1.0%. At higher concentrations, the active sites become saturated, leading to the observed decrease. On the other hand, the capacity of adsorption (mg/g) increased with

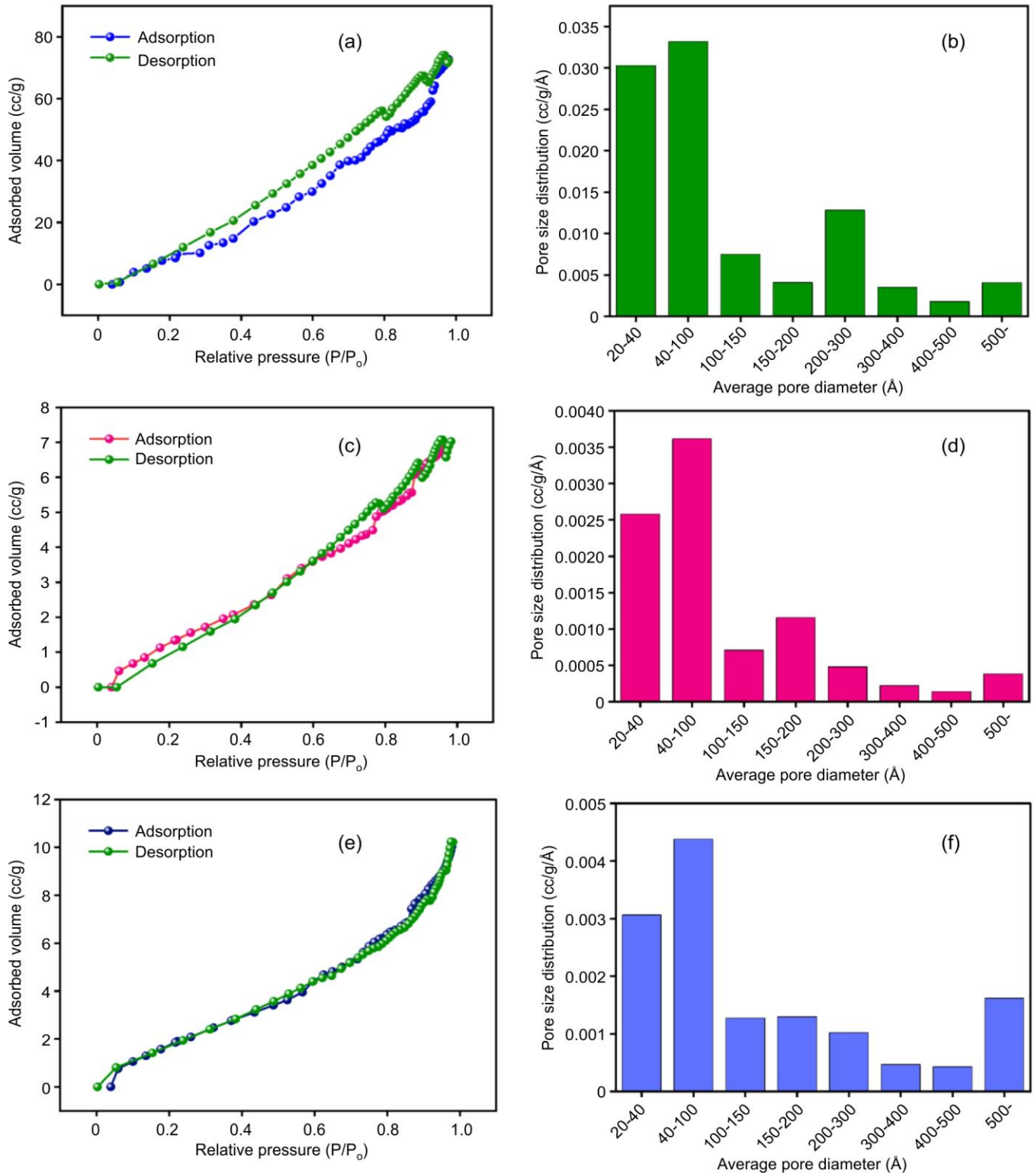

Fig. 4. Nitrogen adsorption-desorption isotherms and pore size distributions of the prepared biosorbents: (a,b) sugarcane bagasse, (c,d) rice husk and (e,f) tea waste

higher initial dye concentrations, with SCB rising from 19.2 ± 0.9 to 45.8 ± 1.2 mg/g, RH from 18.8 ± 0.5 to 44.2 ± 1.1 mg/g and TW from 19.4 ± 0.9 to 43.4 ± 1.1 mg/g. This is due to the higher concentration gradient, which provides a strong thermodynamic driving force that enhances mass transfer and overcomes resistance, facilitating the uptake of crystal violet molecules. As a result, the higher probability of collisions between crystal violet molecules and the adsorbent binding sites leads to increased adsorption capacity [36].

pH of dye solution: Removal efficiency significantly increased for all biosorbents with an increase in pH from 3 to 9. This trend specifies that the adsorption is more effective in

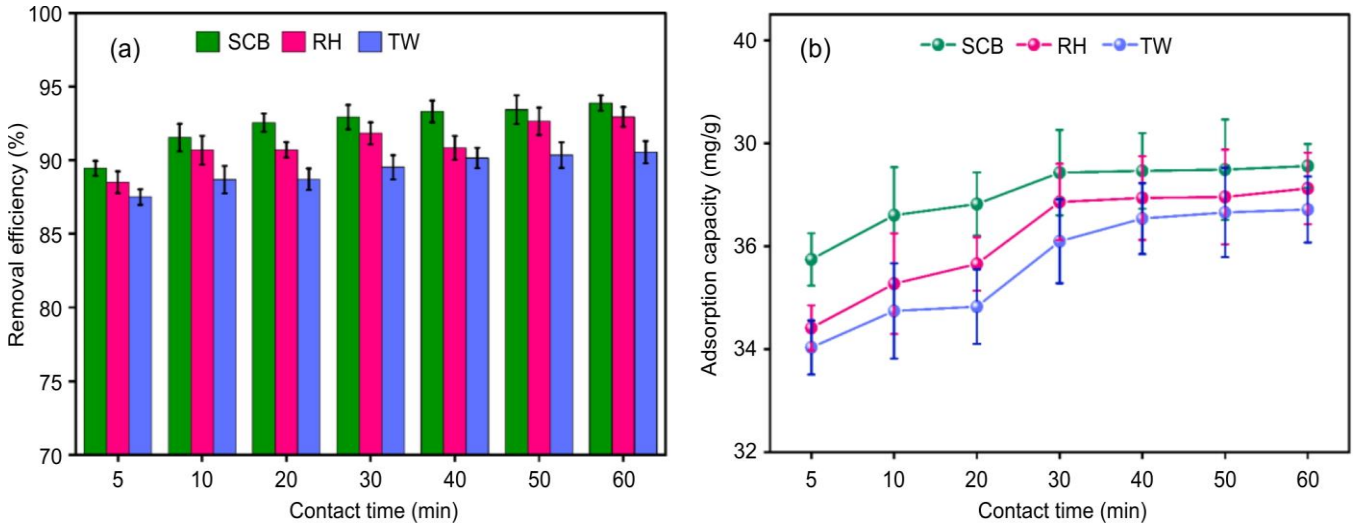

Fig. 5. Effect of contact time on crystal violet adsorption onto biosorbents under the following conditions: w = 1 g/L, C_o = 40 ppm, pH = 9 and T = 303 K; (a) removal efficiency (%) and (b) adsorption capacity (mg/g)

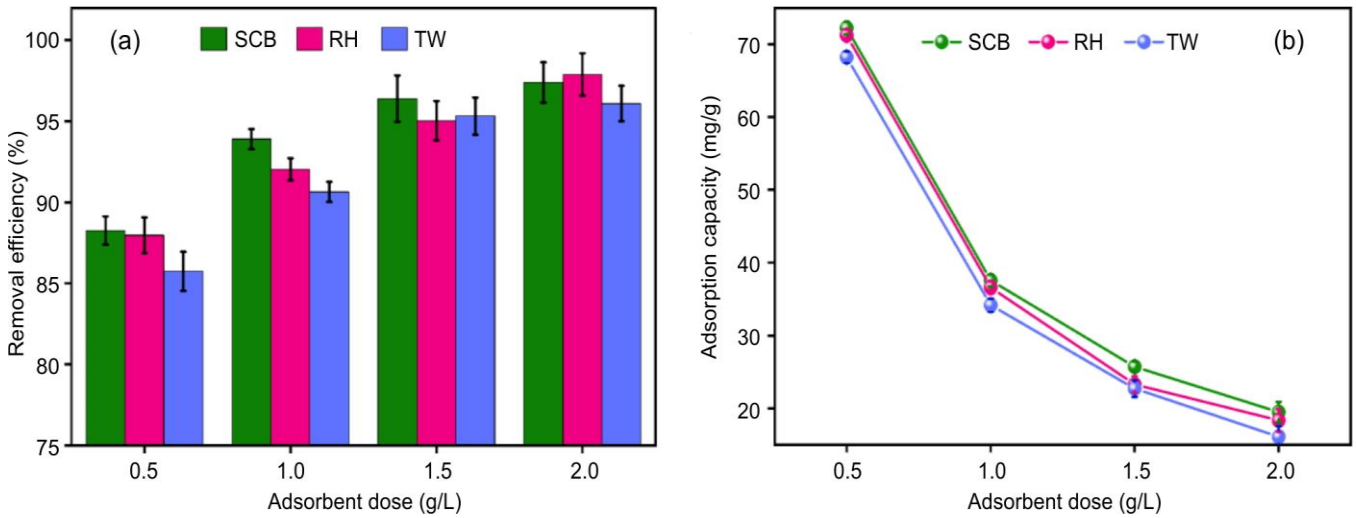

Fig. 6. Effect of biosorbent dosage on the adsorption of crystal violet under the following conditions: t = 40 min, C_o = 40 ppm, pH = 9 and T = 303 K; (a) removal efficiency (%) and (b) adsorption capacity (mg/g)

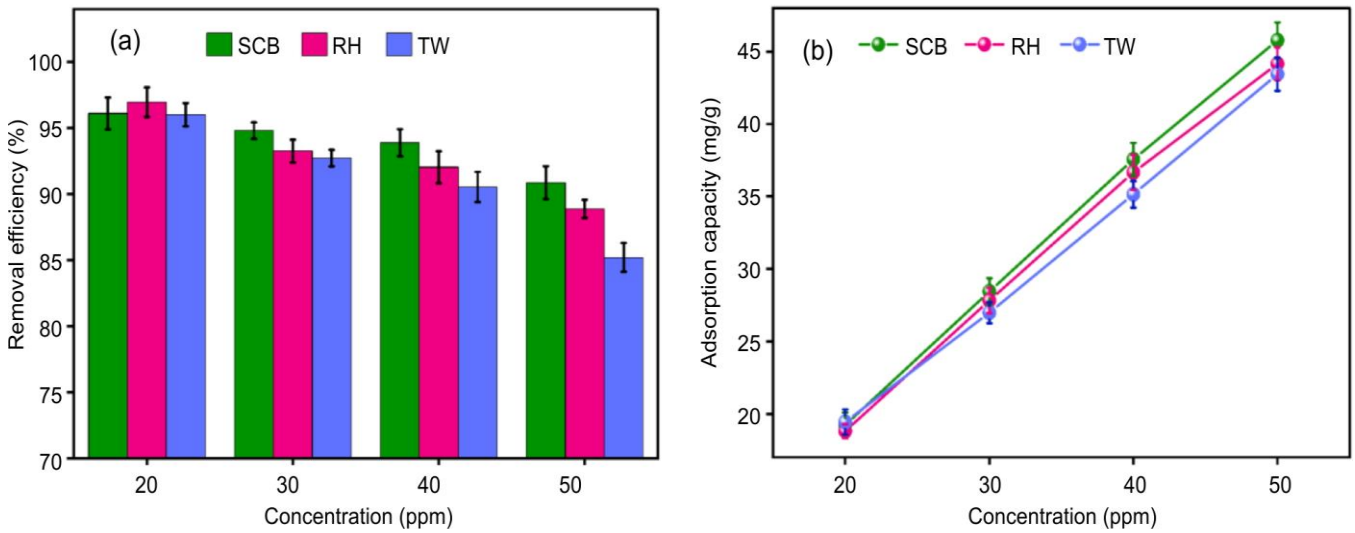

Fig. 7. Effect of initial concentration of crystal violet on (a) removal efficiency (%) and (b) adsorption capacity (mg/g) under conditions: t = 40 min, C_o = 40 ppm, pH = 9 and T = 303 K

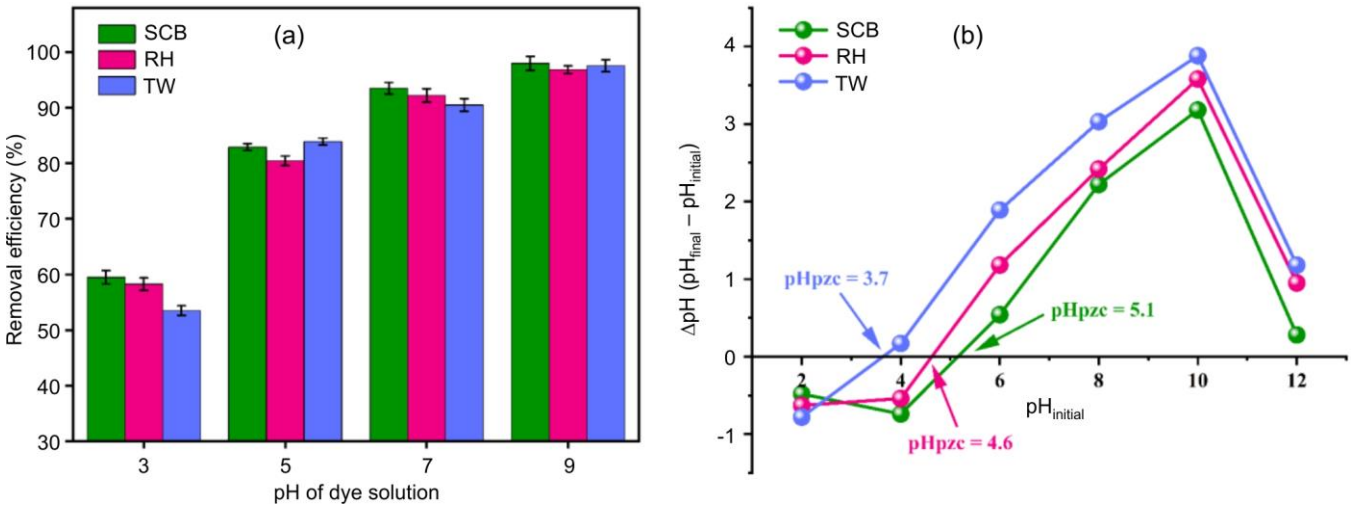

Fig. 8. (a) Effect of pH on the adsorption of crystal violet under conditions: t = 60 min, w = 1 g/L, C_o = 40 ppm and T = 303 K; (b) point of zero charges (pHpzc) of the biosorbents

alkaline conditions (Fig. 8). The pHpzc for SCB, RH and TW was observed at pH 5.1, 4.6 and 3.7, respectively. The biosorbents are expected to have a net positive charge below these values and a net negative charge above them [39]. The rise in pH improved crystal violet adsorption by increasing the biosorbent's surface negativity, thereby strengthening electrostatic interactions with the cationic dye molecules. Previous studies also demonstrate that crystal violet (CV) adsorption on biosorbents improves with higher pH levels [40,41]. At lower pH levels, the biosorbent surface becomes positively charged, leading to competition between excess H^+ ions and CV^+ dye cations for active sites, thereby reducing crystal violet uptake [42]. Therefore, the optimal pH for the experiments was identified as 9.

Temperature of dye solution: The removal efficiency of all the three biosorbents decreased with increasing temperature (303-333 K), implying that crystal violet adsorption is more efficient at lower temperatures (Fig. 9). This trend suggests an exothermic nature of adsorption, where increasing temperature diminishes the binding affinity between crystal violet and the biosorbents, likely by disrupting the physical bonds formed at the adsorbent surface. Consequently, 303 K was chosen as an optimal temperature for further experiments [39].

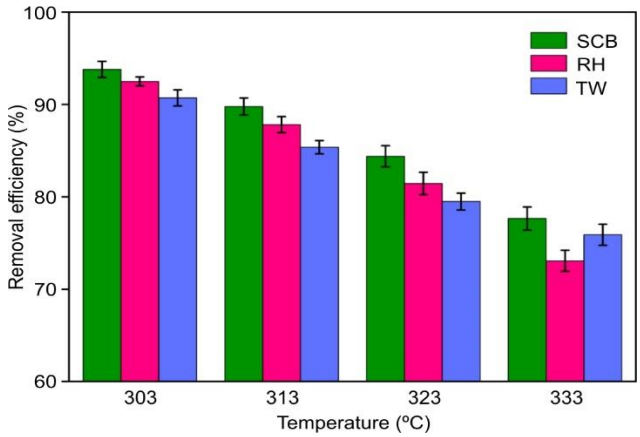

Fig. 9. Effect of temperature on crystal violet adsorption under conditions: t = 60 min, w = 1 g/L, C_o = 40 ppm and pH = 9

Adsorption isotherms: Adsorption isotherms are crucial for examining the interactions between the adsorbent and dye molecules, along with insights into the process's feasibility, nature and adsorption characteristics [23]. The equilibrium data obtained in this study were fitted to Langmuir, Freundlich, Temkin and Dubinin–Radushkevich isotherm models.

According to the Langmuir model, monolayer adsorption occurs on a homogeneous adsorbent surface. Each adsorption site can be occupied by only one dye molecule, disallowing any further adsorption at that location [43]. The Langmuir isotherm in its linear form is expressed as follows [9]:

$$\frac{C_e}{q_e} = \frac{C_e}{q_m} + \frac{1}{K_L q_m} \quad (7)$$

in which q_e indicates the equilibrium adsorption capacity, C_e the equilibrium dye concentration, q_m the maximum capacity of the adsorbent and K_L is the Langmuir adsorption constant. A plot of C_e/q_e against C_e is used to obtain the values of q_m and K_L, which results in a linear graph characterized by a slope of $1/q_m$ and an intercept of $1/K_L q_m$ [11].

The term R_L is called the separation factor, indicates adsorption favourability onto the biosorbents and is calculated using the following equation [44]:

$$R_L = \frac{1}{1 + K_L C_o} \quad (8)$$

The characteristics of the adsorption process are revealed through the interpretation of R_L values, as shown below [45]:

The Freundlich isotherm model, expressed as an empirical model, describes adsorption involving multiple layers on surfaces that are not uniform [46]. According to the model, an increase in adsorbate concentration leads to a corresponding increase in the amount adsorbed on the adsorbent surface. Adsorption initially occurs at sites with higher binding energy, then extends to lower-energy sites, leading to an exponential decrease in adsorption strength until equilibrium is achieved [43]. The linear form of the Freundlich isotherm equation can be expressed as follows:

$$\ln q_e = \ln K_F + \frac{1}{n}(\ln C_e) \quad (9)$$

where 1/n represents the intensity of adsorption and K_F is the Freundlich constant. These parameters are derived from the slope and intercept of a ln q_e *vs.* ln C_e plot. The value of 1/n determines the nature of adsorption: favourable (0 < 1/n < 1) or unfavourable (1/n > 1) [46].

The Temkin isotherm considers the interactions between the adsorbate and adsorbent, assuming that the heat of adsorption decreases linearly as surface coverage increases. Unlike the Langmuir and Freundlich models, which focus on homogeneous and heterogeneous surfaces, respectively, the Temkin model suggests that the adsorption energy distribution decreases uniformly as the adsorbate molecules occupy the surface [47]. The linear equation of the Temkin model is:

$$q_e = \frac{RT}{b}\ln K_T + \frac{RT}{b}\ln C_e \quad (10)$$

where K_T represents the equilibrium binding constant and b indicates the adsorption heat. These constants are determined by plotting q_e against ln C_e. The value of b lower than 8 kJ/mol indicates a physisorption process involving weaker forces like van der Waals interactions and hydrogen bonding. In contrast, when the b value exceeds 8 kJ/mol, it indicates chemisorption, where stronger chemical interactions, such as covalent or ionic bonds, are formed between the adsorbate and adsorbent [47].

The Dubinin–Radushkevich (D–R) model is commonly used to distinguish between physical and chemical adsorption by evaluating the associated energy. Unlike the Langmuir isotherm, it does not predict a homogeneous surface or a constant adsorption potential [23,28]. The linearized form of the D–R model can be expressed as [11]:

$$\ln q_e = \ln q_m - \beta\varepsilon^2 \quad (11)$$

where, q_m denotes the theoretical saturation capacity, β denotes the constant related to the adsorption energy and ε^2 denotes the Polanyi potential, determined by as [49]:

$$\varepsilon = RT\ln\left(1+\frac{1}{C_e}\right) \quad (12)$$

where R is the universal gas constant (kJ/mol K), T is the temperature (K) and C_e is the equilibrium concentration of the adsorbate in solution (mg/L). The D–R model helps to estimate the mean free energy of adsorption (E), which is calculated as [47]:

$$E = \left(\frac{1}{2\beta}\right)^{1/2} \quad (13)$$

The value of E is typically employed to identify whether the adsorption process is physical or chemical in nature [50].

Fig. 10 presents the linear plots corresponding to the applied isotherm models. The parameters obtained from each isotherm model and their respective correlation coefficients (R^2 values), are summarized in Table-3. Maximum adsorp-

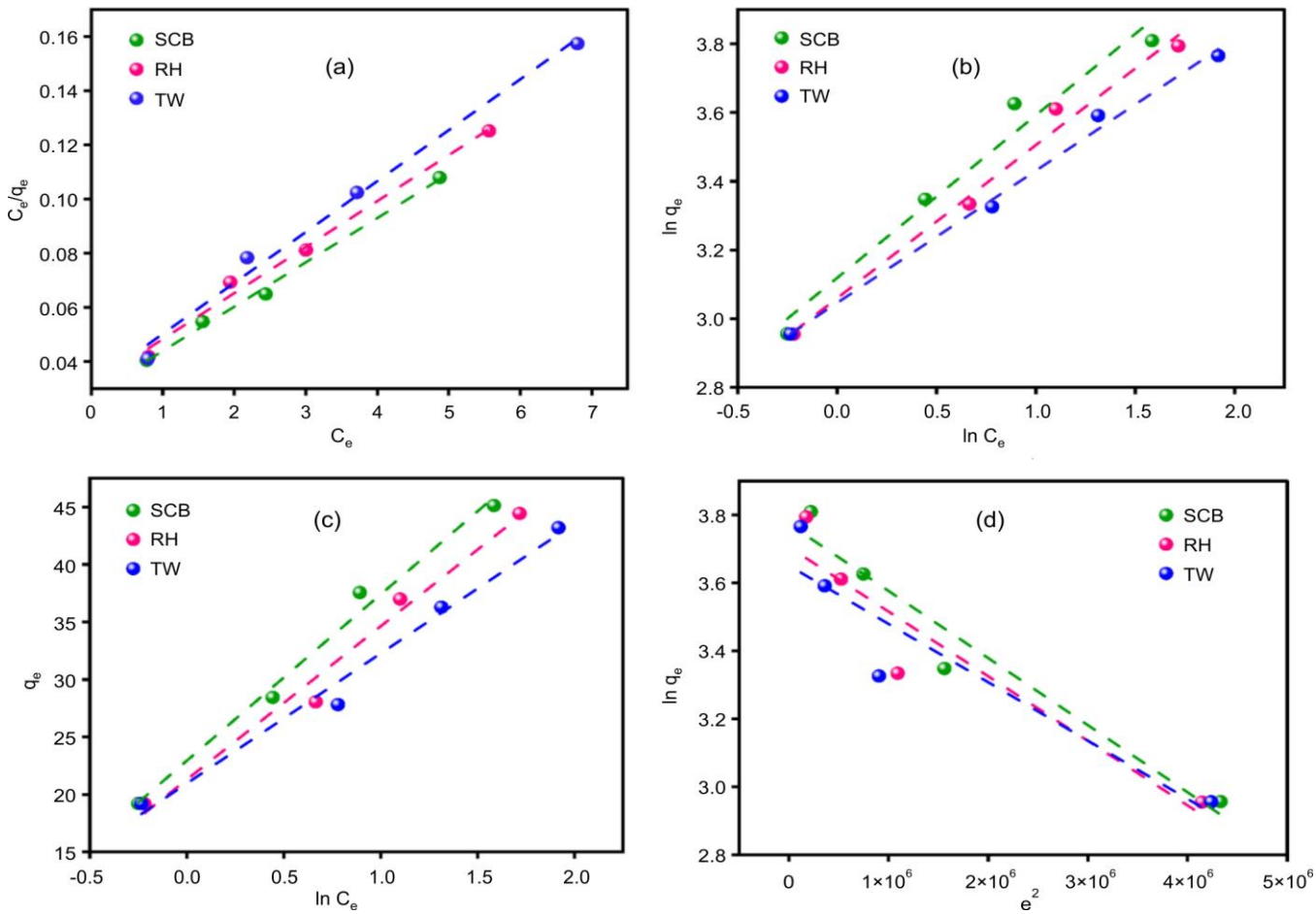

Fig. 10. Adsorption isotherm models for crystal violet adsorption: (a) Langmuir isotherm, (b) Freundlich isotherm, (c) Temkin isotherm and (d) Doubinin-Radushkevich isotherm

TABLE-3
ISOTHERM PARAMETERS FOR CRYSTAL VIOLET ADSORPTION ONTO THE BIOSORBENTS

Model	Parameter	Value		
		SCB	RH	TW
Langmuir	q_m (mg/g)	61.35	58.82	53.19
	K_L (L/mg)	0.59	0.30	0.60
	R_L	0.041	0.077	0.040
	R^2	0.9961	0.99	0.9907
	RMSE	0.848	7.727	1.596
Freundlich	K_F (mg/g)	1314.01	1146.57	1111.48
	1/n	0.474	0.446	0.385
	R^2	0.9686	0.9871	0.9937
	RMSE	1951.16	1773.05	1706.16
Temkin	b (J/mol)	75.602	82.032	96.793
	K_T (L/mg)	1.037	1.037	1.037
	R^2	0.9886	0.9826	0.984
	RMSE	15.59	13.68	13.19
Dubinin-Radushkevich	q_m (mg/g)	43.545	40.674	38.509
	β (mol^2/J^2)	2.00E-07	2.00E-07	2.00E-07
	E (kJ/mol)	1.581	1.581	1.581
	R^2	0.9478	0.8926	0.8707
	RMSE	11.52	12.08	12.23

tion capacities (q_m) estimated using the Langmuir model were 61.35 mg/g, 58.82 mg/g and 53.19 mg/g for SCB, RH and TW, respectively. Values of R_L ($0 < R_L < 1$) reflect the favourable adsorption of crystal violet onto the biosorbents. Similarly, the Freundlich model confirms the favourability of the process with $0 < 1/n < 1$, suggesting efficient adsorption. The heat of adsorption constants (b) calculated from the Temkin model indicate that the adsorption mechanism is primarily physical. The mean free energy (E) calculated from the D–R model further supports this conclusion.

The high R^2 values observed across all four isotherm models indicate the presence of effective monolayer adsorption on homogeneous surfaces, as supported by the Langmuir model and significant multilayer adsorption on heterogeneous surfaces, as described by the Freundlich model. Also, the good fit of the Temkin model indicates strong interactions between the adsorbent and adsorbate, while the D–R model suggests that physical adsorption also plays a role. These adsorption mechanisms were further confirmed through error analysis, including the root mean square error (RMSE), as per eqn. 14:

$$RMSE = \sqrt{\frac{1}{n}\sum_{i=1}^{n}(q_{e,exp} - q_{e,calc})^2} \quad (14)$$

Among all models, the Langmuir model displayed the lowest error values, reinforcing its superior agreement with experimental data and confirming that monolayer adsorption on the homogeneous surfaces of the biosorbents is the main mechanism [11].

Kinetics of adsorption: Adsorption kinetics plays a vital role in designing an effective adsorption system, as it provides insight into the underlying mechanisms and pathways involved in the process [46]. To assess the adsorption rate constants and control mechanisms of crystal violet dye on low-cost biosorbents, four kinetic models were analyzed: pseudo-first-order (PFO), pseudo-second-order (PSO), Elovich and intraparticle diffusion (IPD).

According to the PFO model, the rate of adsorption depends on the gap between the equilibrium adsorption capacity and the amount adsorbed at any moment. This model can be represented in its linear form as [9]:

$$\log(q_e - q_t) = \log q_e - \frac{k_1 t}{2.303} \quad (15)$$

where q_e is the adsorbed amount of crystal violet at equilibrium, q_t is the adsorbed amount of crystal violet at time t and k_1 is the rate constant.

According to the PSO model, the adsorption process is controlled by chemisorption, where electrons are shared or exchanged between the adsorbate and adsorbent [23]. This model can be expressed linearly as [43]:

$$\frac{1}{q_t} = \frac{1}{k_2 q_e^2} + \frac{t}{q_e} \quad (16)$$

where k_2 is the rate constant of pseudo-second order adsorption.

The Elovich model is commonly applied to the chemisorption-based adsorption processes in which the rate of adsorption drops exponentially as adsorption sites are progressively occupied. It is beneficial for heterogeneous surfaces where the energy of adsorption varies across the adsorbent. The model can be formulated in linear terms as [43]:

$$q_t = \frac{1}{\beta}\ln t + \frac{1}{\beta}\ln(\alpha\beta) \quad (17)$$

where α is the adsorption rate at t = 0 (mg/g min) and β is the desorption constant (g/mg).

The linear plots of applied kinetic models are shown in Fig. 11 and the kinetic parameters of each model are presented in Table-4. Based on the highest R^2 values and lowest RMSE, the adsorption of crystal violet onto the biosorbents aligns most closely with the pseudo-second-order model. This indicates the adsorption process is primarily governed by chemisorption, driven by electrostatic interactions between

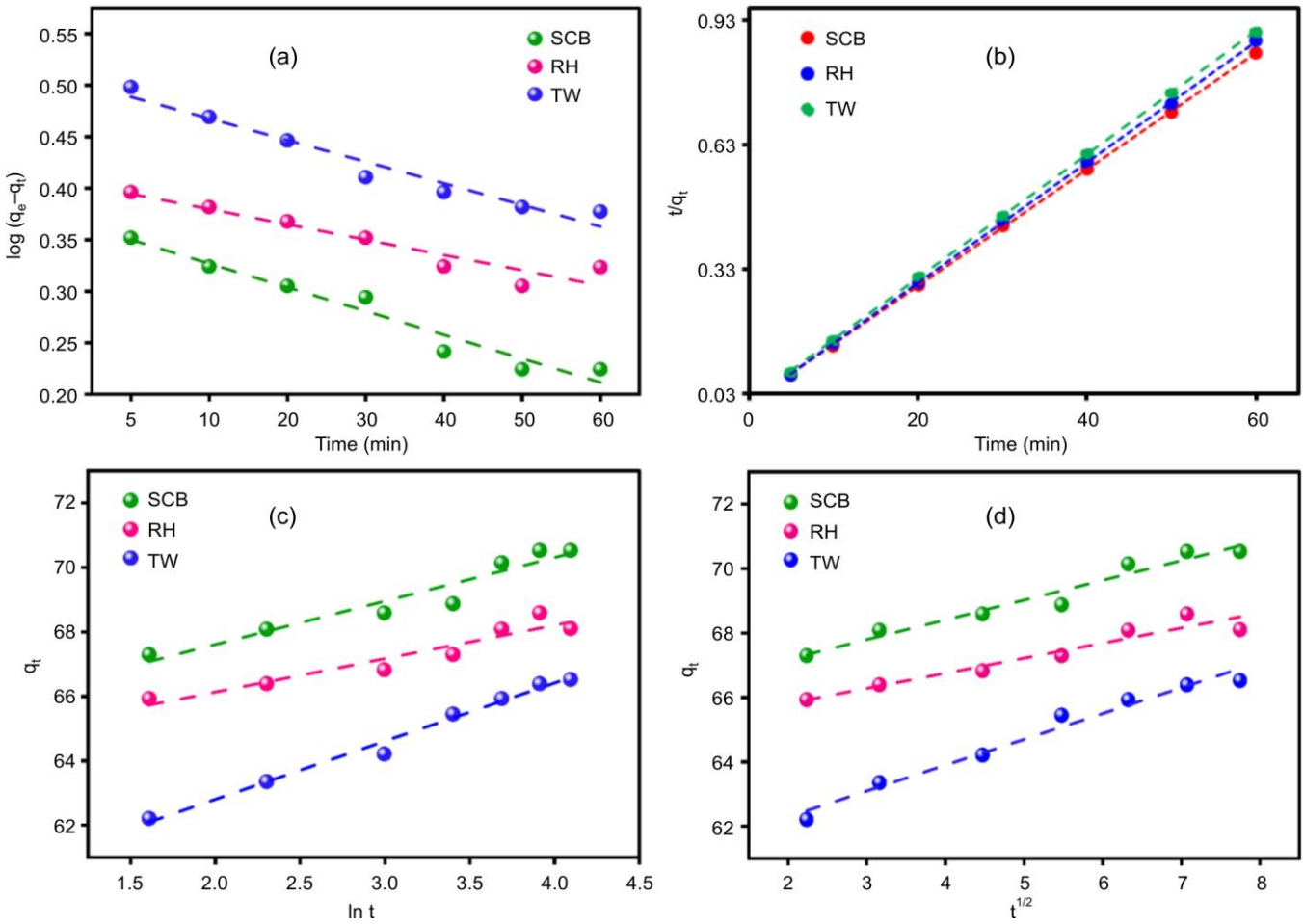

Fig. 11. Adsorption kinetic models for crystal violet adsorption: (a) pseudo-first-order, (b) pseudo-second-order, (c) Elovich and (d) intraparticle-diffusion

TABLE-4
PARAMETERS DESCRIBING THE ADSORPTION KINETICS OF CRYSTAL VIOLET ON THE BIOSORBENTS

Model	Parameter	Value		
		SCB	RH	TW
Experimental data	$q_{e,\,exp}$ (mg/g)	72.21	70.21	68.91
Pseudo-first-order	k_1 (min^{-1})	0.0055	0.0037	0.0051
	$q_{e,\,calc}$ (mg/g)	2.27	2.50	3.11
	R^2	0.945	0.891	0.932
	RMSE	69.937	67.941	66.642
Pseudo-second-order	k_2 (g/(mg min))	0.0269	0.0395	0.0234
	$q_{e,\,calc}$ (mg/g)	70.92	68.49	67.11
	R^2	0.999	0.999	0.999
	RMSE	1.287	0.709	2.008
Elovich	α (mg/(g min))	1.04E+21	6.97E+26	3.07E+14
	β (mg/g)	0.7409	0.9643	0.5536
	R^2	0.922	0.906	0.9874
Intra-particle diffusion	k_{id} ($mg/(g\cdot min^{0.5})$)	0.6137	0.4683	0.8015
	C	65.952	64.876	60.689
	R^2	0.956	0.927	0.976

the biosorbents and dye molecules [51]. The high R^2 values observed for the Elovich model further support this conclusion.

The kinetic data were further examined using the IPD model. This model helps pinpoint the rate-determining stage of adsorption, precisely when the adsorbate diffuses into the adsorbent pores. It helps to determine whether external mass transfer, surface adsorption or intra-pore diffusion predominantly governs the adsorption mechanism. This model can be represented in its linear equation as [51]:

$$q_t = k_{id} t^{1/2} + C \quad (18)$$

with k_{id} denoting the intraparticle diffusion rate constant, $t^{1/2}$ represents half-reaction time and C is the boundary layer thickness.

When a linear plot of q_t against $t^{1/2}$ passes through the origin, IPD is considered the sole rate-controlling step [11,47]. However, as illustrated in Fig. 11d, the regression line does not intersect the origin. So, IPD is not the only rate-limiting mechanism and the boundary layer diffusion also influences the adsorption process [32].

Thermodynamic studies: Thermodynamic analysis of adsorption experiments is crucial to determine spontaneity and feasibility [52]. Therefore, the adsorption data are used to measure enthalpy change (ΔH^o), entropy change (ΔS^o), Gibbs free energy change (ΔG^o) and activation energy (E_a).

The change in enthalpy (ΔH^o) provides valuable information regarding the adsorption process and the van't Hoff equation is usually used to determine it [52].

$$\ln K_d = -\frac{\Delta H^o}{R}\frac{1}{T} + \frac{\Delta S^o}{R} \quad (19)$$

where $K_d = q_e/C_e$ is the distribution coefficient; q_e is the adsorption capacity at equilibrium; and C_e is the dye concentration at equilibrium. A negative ΔH^o indicates that the biosorption process is exothermic and prefers the lower temperatures [27]. Similarly, a positive ΔH^o signifies an endothermic process requiring energy input. Moreover, the magnitude of ΔH^o provides insights into the nature of the adsorption process. The range of ΔH^o values for physical adsorption is between 2.1 and 20.9 kJ/mol, whereas for chemical adsorption, it lies between 80 and 200 kJ/mol [53]. Change in entropy (ΔS^o) can also be determined from the vant' Hoff equation, where a positive ΔS^o provides evidence about the affinity between the adsorbent and adsorbate. It also indicates increased randomness at the interface with structural modifications during adsorption [52].

The spontaneity and feasibility of the adsorption process are assessed through the change in Gibbs free energy (ΔG^o). A negative ΔG^o signifies a spontaneous process, while a positive ΔG^o denotes non-spontaneity [52]. The ΔG^o is usually linked to the equilibrium constant *via* the fundamental Gibbs equation [32].

$$\Delta G^o = -RT\ln K_d = \Delta H^o - T\Delta S^o \quad (20)$$

The activation energy (E_a) represents the minimum energy required to initiate a chemical reaction. The values of E_a suggest the type of adsorption to be either physical (E_a < 40 kJ/mol) or chemical (E_a > 40 kJ/mol) [54]. It can be determined using the following linearized Arrhenius equation [54]:

$$\ln K_2 = -\frac{E_a}{R}\times\frac{1}{T} + \ln A \quad (21)$$

Where k_2 is the PSO rate constant, A is the Arrhenius constant and R is the universal gas constant (8.314 J/mol K).

Fig. 12 illustrates the thermodynamic plots for adsorption and the derived parameters are tabulated in Table-5. The adsorption process is confirmed to be exothermic based on the negative ΔH^o values obtained. Moreover, the values of ΔH^o lie between 2.1 and 20.9 kJ/mol, suggesting that the adsorption primarily involves physisorption. The findings are consistent with the results derived from isotherm models. The negative ΔS^o values suggest a less random configuration of dye molecules on the biosorbent surface, indicating a predo-

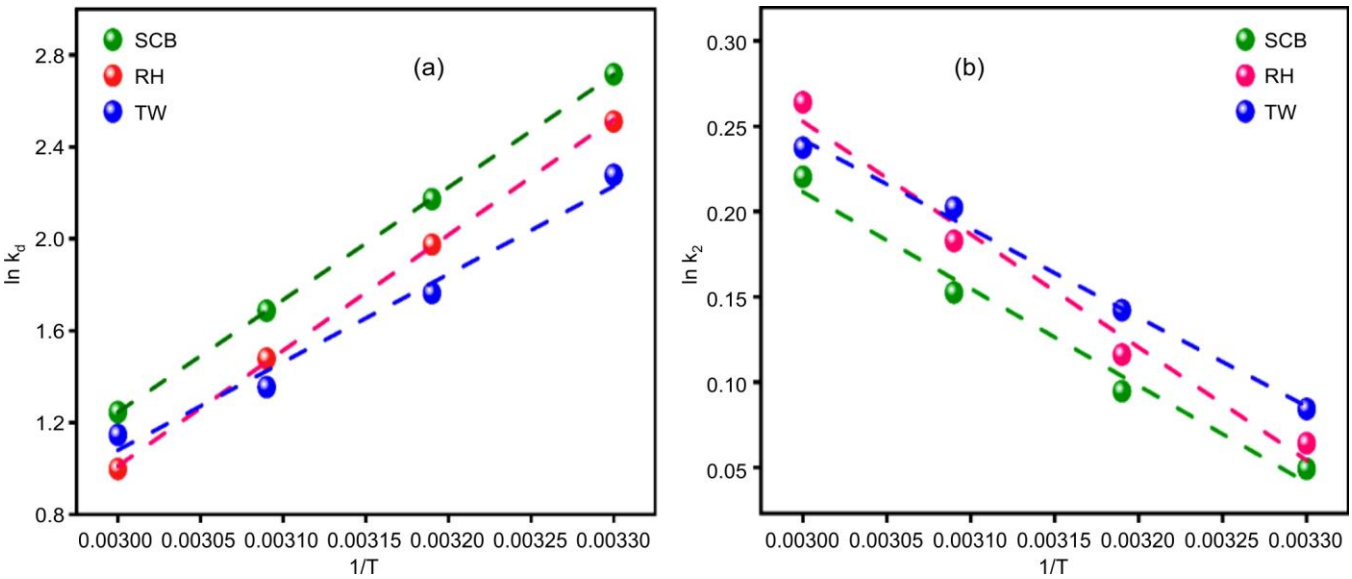

Fig. 12. Thermodynamic analysis of crystal violet adsorption: (a) plot of ln k_d *vs.* 1/T, (b) plot of ln k_2 *vs.* 1/T

TABLE-5
THERMODYNAMIC PARAMETERS FOR CRYSTAL VIOLET ADSORPTION AT VARYING TEMPERATURES

Biosorbent	ΔH^o (kJ/mol)	ΔS^o (kJ/mol/K)	E_a (kJ/mol)	ΔG^o (kJ/mol)			
				303 K	313 K	323 K	333 K
SCB	-41.15	-0.11	-41.12	-6.82	-5.69	-4.56	-3.43
RH	-42.27	-0.12	-40.95	-6.33	-5.15	-3.96	-2.78
TW	-32.10	-0.09	-40.79	-5.59	-4.72	-3.85	-2.97

TABLE-6
MAXIMUM ADSORPTION CAPACITY (q_m) OF VARIOUS LOW-COST AND GREEN BIOSORBENTS

Adsorbent	Dye	q_m (mg/g)	pH	Temperature (ºC)	Ref.
Sagaun sawdust	Crystal violet	4.26	7.5	30	[56]
Neem sawdust	Crystal violet	4.44	7.2	30	[57]
Coniferous pinus bark powder	Crystal violet	32.78	8	30	[58]
Jackfruit leaf powder	Crystal violet	43.40	7	30	[59]
Terminalia arjuna sawdust waste	Crystal violet	45.99	7	30	[36]
Orange peel	Methylene blue	5.87	–	–	[60]
Banana peel	Methylene blue	18.647	8	30	[61]
Rice bran	Methylene blue	20.29	6	20	[62]
Wheat bran	Methylene blue	54.79	6	20	[62]
Sugarcane bagasse	Crystal violet	61.35	9	30	Present work
Rice husk	Crystal violet	58.82	9	30	Present work
Tea waste	Crystal violet	53.19	9	30	Present work

minantly physical adsorption mechanism [53]. The negative ΔG^o values demonstrate that the adsorption of crystal violet onto biosorbents occurs spontaneously, without requiring the external energy. However, as temperature increases, the decreasing values of ΔG^o imply that biosorption becomes less favourable at higher temperatures [55]. The values of activation energy (E_a) were found to be less than 40 kJ/mol for all biosorbents, indicating that the adsorption followed the physisorption mechanism.

Comparative studies: The adsorption capacity of various types of biosorbents varies depending on their primary source, adsorption conditions and the type of contaminant being removed. Widespread research has been conducted to identify the low-cost adsorbents with high adsorption efficiency. So, the present study compares the adsorption capacities of sugarcane bagasse, rice husk and tea waste with those of other low-cost and green adsorbents, as summarized in Table-6. The results indicate that SCB, RH and TW demonstrate superior adsorption capacities compared to other biosorbents reported in the literature.

Conclusion

This study demonstrates the effectiveness of sugarcane bagasse (SCB), rice husk (RH) and tea waste (TW) as cost-efficient biosorbents for removing crystal violet dye from aqueous environments. The best adsorption performance was observed under conditions of 1 g/L biosorbent dosage, 40 ppm initial dye concentration, pH 9 and 30 ºC solution temperature. Among the biosorbents, SCB exhibited superior adsorption capacity, resulting from its larger surface area, greater pore volume and a variety of functional groups. The equilibrium data were well-aligned by the Langmuir isotherm, with maximum adsorption capacities of 61.35, 58.82 and 53.19 mg/g for SCB, RH and TW, respectively. The adsorption kinetics fitted with the PSO model, indicating the potential role of chemical interactions. Thermodynamic parameters and activation energy analyses confirmed the adsorption process to be endothermic and predominantly driven by physisorption. These findings underscore the potential of SCB, RH and TW as green, cost-effective and efficient biosorbents for dye removal in wastewater treatment. Future research should focus on assessing their regeneration and reusability, performance in real wastewater systems and sustainability through environmental toxicity and life cycle analyses.

ACKNOWLEDGEMENTS

The Mawlana Bhashani Science and Technology University (MBSTU) Research cell partially supported this research in the Fiscal years 2023-2024 and 2024-2025.

CONFLICT OF INTEREST

The authors declare that there is no conflict of interests regarding the publication of this article.

REFERENCES

1. F. Westall and A. Brack, *Space Sci. Rev.*, **214**, 50 (2018); https://doi.org/10.1007/s11214-018-0476-7
2. H. Shemer, S. Wald, and R. Semiat, *Membranes*, **13**, 612 (2023); https://doi.org/10.3390/membranes13060612
3. A. Ayele, D. Getachew, M. Kamaraj and A. Suresh, *J. Chem.*, **2021**, 9923643 (2021); https://doi.org/10.1155/2021/9923643
4. Aruna, N. Bagotia, A.K. Sharma and S. Kumar, *Chemosphere*, **268**, 129309 (2021); https://doi.org/10.1016/j.chemosphere.2020.129309
5. R. Foroutan, S.J. Peighambardoust, S.H. Peighambardoust, M. Pateiro and J.M. Lorenzo, *Molecules*, **26**, 2241 (2021); https://doi.org/10.3390/molecules26082241
6. S. Pashaei-Fakhri, S.J. Peighambardoust, R. Foroutan, N. Arsalani and B. Ramavandi, *Chemosphere*, **270**, 129419 (2021); https://doi.org/10.1016/j.chemosphere.2020.129419
7. H. Mittal, A. Al Alili, P.P. Morajkar and S.M. Alhassan, *J. Mol. Liq.*, **323**, 115034 (2021); https://doi.org/10.1016/j.molliq.2020.115034
8. V. Katheresan, J. Kansedo and S.Y. Lau, *J. Environ. Chem. Eng.*, **6**, 4676 (2018); https://doi.org/10.1016/j.jece.2018.06.060
9. H. Jain, V. Yadav, V.D. Rajput, T. Minkina, S. Agarwal and M.C. Garg, *Water Air Soil Pollut.*, **233**, 187 (2022); https://doi.org/10.1007/s11270-022-05655-0
10. N. Shafiq, A.A.E. Hussein, M.F. Nuruddin and H. Al Mattarneh, *Proc. Inst. Civ. Eng., Eng. Sustain.*, **171**, 123 (2018); https://doi.org/10.1680/jensu.15.00014
11. M. Saidul Islam Ropak, F. Yasmin, M.A. Rahaman and U. Salma, *Colloids Surf. A Physicochem. Eng. Asp.*, **704**, 135477 (2025); https://doi.org/10.1016/j.colsurfa.2024.135477
12. Alokika, Anu, A. Kumar, V. Kumar and B. Singh, *Int. J. Biol. Macromol.*, **169**, 564 (2021); https://doi.org/10.1016/j.ijbiomac.2020.12.175
13. K.T. Tong, R. Vinai and M.N. Soutsos, *J. Clean. Prod.*, **201**, 272 (2018); https://doi.org/10.1016/j.jclepro.2018.08.025
14. B. Debnath, D. Haldar and M.K. Purkait, *J. Environ. Chem. Eng.*, **9**, 106179 (2021); https://doi.org/10.1016/j.jece.2021.106179

15. D.H.K. Reddy, K. Seshaiah, A.V.R. Reddy, M.M. Rao and M.C. Wang, *J. Hazard. Mater.*, **174**, 831 (2010); https://doi.org/10.1016/j.jhazmat.2009.09.128
16. P.L. Homagai, R. Poudel, S. Poudel and A. Bhattarai, *Heliyon*, **8**, e09261 (2022); https://doi.org/10.1016/j.heliyon.2022.e09261
17. Z. Jiang and D. Hu, *J. Mol. Liq.*, **276**, 105 (2019); https://doi.org/10.1016/j.molliq.2018.11.153
18. T. Islam, C. Peng, I. Ali, J. Li, Z.M. Khan, M. Sultan and I. Naz, *Arab. J. Sci. Eng.*, **46**, 233 (2021); https://doi.org/10.1007/s13369-020-04537-z
19. A. Nasar, *Biomass Convers. Biorefin.*, **13**, 1399 (2023); https://doi.org/10.1007/s13399-020-01205-y
20. H.S. Hafid, F.N. Omar, J. Zhu and M. Wakisaka, *Carbohydr. Polym.*, **260**, 117789 (2021); https://doi.org/10.1016/j.carbpol.2021.117789
21. S. Vigneshwaran, M. Uthayakumar and V. Arumugaprabu, *J. Clean. Prod.*, **276**, 124278 (2020); https://doi.org/10.1016/j.jclepro.2020.124278
22. K. Bhandari, S. Roy Maulik and A.R. Bhattacharyya, *J. Inst. Eng. Ser. E*, **101**, 99 (2020); https://doi.org/10.1007/s40034-020-00160-7
23. T. Ullah, H. Gul, F. Khitab, R. Khattak, Y. Ali, S. Rasool, M.S. Khan and I. Zekker, *Water*, **14**, 3014 (2022); https://doi.org/10.3390/w14193014
24. T.E. Abilio, B.C. Soares, J.C. José, P.A. Milani, G. Labuto and E.N.V.M. Carrilho, *Environ. Sci. Pollut. Res. Int.*, **28**, 24816 (2021); https://doi.org/10.1007/s11356-020-11726-8
25. M. Gun, H. Arslan, M. Saleh, M. Yalvac and N. Dizge, *Int. J. Environ. Res.*, **16**, 20 (2022); https://doi.org/10.1007/s41742-022-00399-5
26. L. Liu, S. Fan and Y. Li, *Int. J. Environ. Res. Public Health*, **15**, 1321 (2018); https://doi.org/10.3390/ijerph15071321
27. U. Kamran, H.N. Bhatti, S. Noreen, M.A. Tahir and S.J. Park, *Chemosphere*, **291**, 132796 (2022); https://doi.org/10.1016/j.chemosphere.2021.132796
28. X. Fan, L. Deng, K. Li, H. Lu, R. Wang and W. Li, *Colloid Interface Sci. Commun.*, **44**, 100485 (2021); https://doi.org/10.1016/j.colcom.2021.100485
29. T.-H. Liou and Y.H. Liou, *Materials*, **14**, 1214 (2021); https://doi.org/10.3390/ma14051214
30. M. Bansal, P.K. Patnala and T. Dugmore, *Curr. Res. Green Sustain. Chem.*, **3**, 100036 (2020); https://doi.org/10.1016/j.crgsc.2020.100036
31. A. Ebrahimian and E. Saberikhah, *Cellul. Chem. Technol.*, **47**, 657 (2013).
32. F. Batool, S. Kanwal, H. Kanwal, S. Noreen, M.S. Hodhod, M. Mustaqeem, G. Sharif, H.K. Naeem, J. Zahid and A.R.Z. Gaafar, *Molecules*, **28**, 7124 (2023); https://doi.org/10.3390/molecules28207124
33. F. Naseeruteen, N.S.A. Hamid, F.B.M. Suah, W.S.W. Ngah and F.S. Mehamod, *Int. J. Biol. Macromol.*, **107**, 1270 (2018); https://doi.org/10.1016/j.ijbiomac.2017.09.111
34. J. Wang, Z. Zhang, D. He, H. Yang, D. Jin, J. Qu and Y. Zhang, *Sustainability*, **12**, 8335 (2020); https://doi.org/10.3390/su12208335
35. H. Li, H. Jin, R. Li, J. Hua, Z. Zhang and R. Li, *Sci. Rep.*, **14**, 1217 (2024); https://doi.org/10.1038/s41598-023-50368-x
36. S. Shakoor and A. Nasar, *Groundw. Sustain. Dev.*, **7**, 30 (2018); https://doi.org/10.1016/j.gsd.2018.03.004
37. A.E. Ahmed and K. Majewska-Nowak, *Environ. Prot. Eng.*, **47**, 109 (2020); https://doi.org/10.37190/epe210309
38. N.K. Mondal and S. Kar, *Appl. Water Sci.*, **8**, 157 (2018); https://doi.org/10.1007/s13201-018-0811-x
39. S. El Bourachdi, F. El Ouadrhiri, F. Moussaoui, E.A.M. Saleh, A. El Amri, R.H. Althomali, A.F. Kassem, M.M. Moharam, A.R. Ayub, K. Husain, I. Hassan and A. Lahkimi, *Int. J. Chem. Eng.*, **2024**, 8222314 (2024); https://doi.org/10.1155/2024/8222314
40. F.Z. Ankouri, H. Lamkhanter, A. Jaafar, Z. Lakbaibi and H. Mountacer, *Chem. Africa*, **6**, 1495 (2023); https://doi.org/10.1007/s42250-022-00579-y
41. A.A. Oladipo, M. Gazi and S. Saber-Samandari, *J. Taiwan Inst. Chem. Eng.*, **45**, 653 (2014); https://doi.org/10.1016/j.jtice.2013.07.013
42. A.A. Inyinbor, F.A. Adekola and G.A. Olatunji, *S. Afr. J. Chem.*, **68**, 115 (2015).
43. L.R. Martins, J.A.V. Rodrigues, O.F.H. Adarme, T.M.S. Melo, L.V.A. Gurgel and L.F. Gil, *J. Colloid Interface Sci.*, **494**, 223 (2017); https://doi.org/10.1016/j.jcis.2017.01.085
44. A. Ghazali, M. Shirani, A. Semnani, V. Zare-Shahabadi and M. Nekoeinia, *J. Environ. Chem. Eng.*, **6**, 3942 (2018); https://doi.org/10.1016/j.jece.2018.05.043
45. H.M.H. Gad and A.A. El-Sayed, *J. Hazard. Mater.*, **168**, 1070 (2009); https://doi.org/10.1016/j.jhazmat.2009.02.155
46. A. Babapoor, O. Rafiei, Y. Mousavi, M.M. Azizi, M. Paar and A. Nuri, *Int. J. Chem. Eng.*, **2022**, 1 (2022); https://doi.org/10.1155/2022/3282448
47. V.S. Munagapati, H.Y. Wen, A.R.K. Gollakota, J.C. Wen, C.M. Shu, K.Y. Andrew Lin, Z. Tian, J.H. Wen, G.M. Reddy and G.V. Zyryanov, *J. Mol. Liq.*, **345**, 118255 (2022); https://doi.org/10.1016/j.molliq.2021.118255
48. S. Tunali, A. Ozcan, Z. Kaynak, A.S. Ozcan and T. Akar, *J. Environ. Sci. Health Part A Tox. Hazard. Subst. Environ. Eng.*, **42**, 591 (2007); https://doi.org/10.1080/10934520701244359
49. Q. Li, Q. Yue, Y. Su, B. Gao, L. Fu, *J. Hazard. Mater.*, **147**, 370 (2007); https://doi.org/10.1016/j.jhazmat.2007.01.024
50. D. Parashar and R. Gandhimathi, *Water Air Soil Pollut.*, **233**, 400 (2022); https://doi.org/10.1007/s11270-022-05857-6
51. D. Sana and S. Jalila, *Chin. J. Chem. Eng.*, **25**, 1282 (2017); https://doi.org/10.1016/j.cjche.2017.01.012
52. A.N. Ebelegi, N. Ayawei and D. Wankasi, *Open J. Phys. Chem.*, **10**, 166 (2020); https://doi.org/10.4236/ojpc.2020.103010
53. E. Wibowo, M. Rokhmat, Sutisna, Khairurrijal and M. Abdullah, *Desalination*, **409**, 146 (2017); https://doi.org/10.1016/j.desal.2017.01.026
54. Y. Erdogan, B. Isik, V. Ugraskan and F. Cakar, *Biomass Convers. Biorefin.*, **14**, 663 (2024); https://doi.org/10.1007/s13399-022-02349-9
55. H.R. Mahmoud, S.M. Ibrahim and S.A. El-Molla, *Adv. Powder Technol.*, **27**, 223 (2016); https://doi.org/10.1016/j.apt.2015.12.006
56. S.D. Khattri and M.K. Singh, *Environ. Prog. Sustain. Energy*, **31**, 435 (2012); https://doi.org/10.1002/ep.10567
57. S.D. Khattri and M.K. Singh, *Water Air Soil Pollut.*, **120**, 283 (2000); https://doi.org/10.1023/A:1005207803041
58. R. Ahmad, *J. Hazard. Mater.*, **171**, 767 (2009); https://doi.org/10.1016/j.jhazmat.2009.06.060
59. P.D. Saha, S. Chakraborty and S. Chowdhury, *Colloids Surf. B Biointerfaces*, **92**, 262 (2012); https://doi.org/10.1016/j.colsurfb.2011.11.057
60. D. Kavitha and C. Namasivayam, *Bioresour. Technol.*, **98**, 14 (2007); https://doi.org/10.1016/j.biortech.2005.12.008
61. K. Amela, M.A. Hassen and D. Kerroum, *Energy Procedia*, **19**, 286 (2012); https://doi.org/10.1016/j.egypro.2012.05.208
62. X.S. Wang, Y. Zhou, Y. Jiang and C. Sun, *J. Hazard. Mater.*, **157**, 374 (2008); https://doi.org/10.1016/j.jhazmat.2008.01.004